Dynamics of a Creeping Newtonian Jet With Gravity and Surface Tension: A Finite Difference Technique for Solving Steady Free-Surface Flows Using Orthogonal Curvilinear Coordinates

A finite difference technique capable of simulating steady, incompressible, viscous, free-surface flows has been successfully applied to the motion of a creeping Newtonian jet, including both surface tension and gravitational forces. In accordance with experimental results, the numerical solutions predict either a 12 or 16% increase in the jet dimensions depending on whether the jet emerges from a circular or a slit die. Both gravity and surface tension inhibit the swelling behavior.

ANIT DUTTA and M. E. RYAN

Department of Chemical Engineering, State University of New York at Buffalo, Amherst, NY 14260

SCOPE

Low Reynolds number flows, associated primarily with the motion of highly viscous liquids such as polymer melts, are commonly encountered in a large variety of industrial processing operations. A particular flow situation of considerable practical and rheological importance, is that of a highly viscous liquid emerging from a conduit (die) into an inviscid medium. The characteristic feature of this flow is that the cross-sectional area of the jet increases as it emerges from the die. Hence, this phenomenon is simply known as "jet swell" or "die swell." The die swell ratio, which is a quantitative measure of the swelling behavior, is the ratio of the final jet dimension to that of the die and has been determined to be strongly dependent on the rheological properties of the liquid. In fact, this ratio varies over a range as wide as 2–3 for viscoelastic liquids (Graessley et al., 1970; Utracki et al., 1975; Huang and White, 1979) to about 1.1–1.2 for Newtonian fluids (Middleman and Gavis, 1961; Goren and Wronski, 1966; Batchelor et al., 1973). Since die swell has a direct influence on the dimensions of the final product in processes like extrusion, fiber spinning, and blow molding, it is necessary to obtain a fundamental understanding of the die swell phenomenon in order to obviate the need to rely on trial and error procedures and to ensure successful design and operation of the process. A basic understanding of the relationship of die swell to material properties and process conditions would permit the realistic assessment and evaluation of the cost effectiveness and profitability of new products and designs.

Apart from the inherent importance to polymer processing, a fundamental knowledge regarding the nonviscometric flow associated with that of a creeping jet is of considerable significance for the successful application of the jet-thrust technique to measure normal stresses. As has been indicated by Davies et al. (1977) for Newtonian liquids and by Boger and Denn (1980) for viscoelastic liquids, the serious discrepancies observed between the normal stress data obtained by the jet-thrust technique and the data obtained by employing standard viscometric flows, are very likely due to the assumption of the viscometric flow being prevalent up to the die exit. Therefore, in order for the jet-thrust technique to be used successfully, it is essential to acquire a detailed understanding of the severe velocity profile and stress rearrangements that occur in the exit region of a creeping jet flow. Since experimental measurements possess formidable practical difficulties, a theoretical analysis of the problem appears to be a viable alternative.

Several theoretical analyses of die swell behavior have been presented in the literature. These mathematical formulations of the die swell problem are based either on a momentum balance approach (Metzner et al., 1961) or on an elastic recovery mechanism (Graessley et al., 1970; Nakajima and Shida, 1966; Tanner, 1970; Bagley and Duffey, 1970; Vlachopoulos et al., 1972; Pearson and Trottnow, 1978). Even though these theories have proven to be somewhat successful, they fail to adequately explain the swelling behavior of a Newtonian fluid. Experimental observations, however, indicate that at low shear rates the die swell behavior of a viscoelastic polymer melt tends to approach that of a Newtonian fluid. Thus, in order to develop a general theory of die swell, an alternative and more satisfactory approach would be to solve the governing equations of motion along with an appropriate constitutive equation in a region including both upstream and downstream sections from the die exit. However, before the more complex problem incorporating Non-Newtonian and viscoelastic fluid behavior is attempted, it is imperative to develop a simple and efficient calculation procedure for the prediction of Newtonian swelling behavior.

The analysis presented here yields a simple finite difference technique for solving steady free-surface flow problems. The usual difficulties associated with the application of a finite difference procedure in an irregularly-shaped flow domain are circumvented in the present analysis by the application of a conformal transformation of the flow region. In particular, the method has been employed to solve the Newtonian jet swell problem including both gravitational and surface tension effects.

ISSN 0001-1541-82-5220-0220-$2.00.

CONCLUSIONS AND SIGNIFICANCE

The numerical solution of the creeping jet flow problem exhibits features which have been observed experimentally. Rapid rearrangement of the flow field occurs as the fluid approaches the die opening. The rearrangement process is essentially complete within a distance of about one die opening both upstream and downstream from the exit plane. Existence of such an exit region has been comfirmed by the recent velocity profile measurements of Higashitani et al. (1976), Whipple and Hill (1978), and Gottlieb and Bird (1979). Moreover, in agreement with the experimental data of Middleman and Gavis (1961) and Batchelor et al. (1973), a Newtonian jet is predicted to expand by as much as 12 or 16% depending on whether the die geometry is cylindrical or planar. Both gravity and surface tension tend to decrease this swelling behavior. The influence of gravity, however, is much more significant than that due to surface tension for determining the final shape of the jet. The striking features of this flow are the presence of pressure and stress singularities which exist at the die exit. A sudden transition occurs from very high shear stresses to even larger tensile stresses at the exit section. It is this aspect of the flow that makes it virtually impossible for numerical solutions to satisfy all the stress conditions and conservation requirements simultaneously at the free surface, particularly in the immediate vicinity of the die exit.

The principal significance of this work is to provide a relatively simple and efficient numerical calculation procedure capable of simulating steady free-surface flows. The method can equally well be applied to flow situations involving arbitrarily-curved solid boundaries. The numerical solutions presented here yield detailed information regarding the complex nature of the flow within the exit region for a fluid exhibiting Newtonian behavior. It is believed that the basic numerical scheme can be extended to simulate the more complex problem of Non-Newtonian jet swell. The inherent simplicity of the finite difference technique makes it an attractive alternative to finite element methods for the analysis of the jet swell phenomenon. As mentioned earlier, a more complete understanding of swelling behavior is of considerable importance for the processing and characterization of polymeric materials.

PREVIOUS NUMERICAL WORK

Practically all of the previous work regarding the numerical solution of a creeping Newtonian jet has been carried out using finite element techniques with the pressure and velocity as variables. The first successful solution of this problem is due to Nickell et al. (1974). Their analysis was subsequently generalized for the case of a power-law constitutive relation by Tanner et al. (1975) and for various upstream die geometries by Allan (1977). Efforts have also been made to extend the computations to higher Reynolds number and to include the effect of surface tension forces. Such calculations have been reported by Reddy and Tanner (1978a) and by Omodei (1980) for axisymmetric jets and by Omodei (1979) and by Ruschak (1980) for plane jets. Furthermore, Silliman and Scriven (1978, 1980) have investigated the influence of a slip boundary condition at the die wall for the case of a plane jet.

For the creeping jet flow of a viscoelastic liquid, the finite element technique has only been successfully used for fluids exhibiting weakly elastic behavior. Reddy and Tanner (1978b) used a second-order fluid model in order to predict the swelling of a plane jet, whereas Chang et al. (1979) employed a non-linear Maxwell model for both axisymmetric and planar geometries. In addition, the latter employed both a Galerkin and a collocation method for the solution of the problem at low, but non-zero, Reynolds number. Recently, Crochet and Kuenings (1980) reported calculations for the die swell of a convected Maxwell fluid using a numerical method of mixed finite element type. In addition to circular and slit dies, these authors also considered the swelling due to an annular die. Here too, numerical results could only be obtained for fluids possessing a relatively small degree of elasticity. All of these studies, however, have neglected the influence of the gravitational field. For a more realistic simulation it would be desirable to incorporate the influence of both surface tension and gravitational forces.

PRESENT APPROACH

Finite difference techniques have been extensively used for the simulation of a wide spectrum of flow situations. Surprisingly, no serious attempts have been made to utilize this numerical procedure for the analysis of the jet swell problem, even though the initial effort of analyzing the Newtonian jet swell phenomenon was undertaken by Horsfall (1973) employing a traditional finite difference numerical scheme. His numerical solution, however, predicted a swell ratio considerably smaller than that observed experimentally. This poor surface determination was probably due to inaccuracies (resulting from interpolation) in enforcing the boundary conditions at the curved free surface.

Since the finite difference approach possesses inherent simplicity of formulation and ease of mesh refinement, which are of particular relevance for problems involving fluids described by complex constitutive relationships, it was deemed appropriate to develop a simple, efficient, finite difference scheme capable of solving steady free-surface flows, in particular, the jet swell problem. The present work, however, is solely concerned with Newtonian fluid behavior. The basic approach is to circumvent the major difficulty of accurate representation of the curved boundary by transformation of the irregularly-shaped flow domain into a rectangular region. Such techniques have been extensively used to solve a wide class of flow problems involving curved solid boundaries (Thom, 1933; Lee and Fung, 1970). The transformation permits the free boundary to be represented by grid nodes in the finite difference mesh, thereby eliminating any need for interpolation. In fact, this transformation procedure permits the finite difference scheme to approach the boundary generality of the finite element methods.

Apart from the difficulties associated with the unknown shape and location of the free surface, another problem arises from the surface boundary conditions which are expressed in terms of stresses. Traditionally, free-surface calculations, employing either finite element or finite difference (Harlow and Welch, 1965) techniques, have employed the velocity and pressure as the primitive variables. For steady flow problems, if the continuity equation is not solved directly along with the momentum equations, this primitive variable formulation poses considerable difficulties in satisfying the mass conservation requirement. On the other hand, if the stream function-vorticity formulation is employed, mass continuity is satisfied identically but difficulties are encountered in enforcing the free-surface boundary conditions involving pressure explicitly. Although the pressure could be eliminated by differentiation and algebraic manipulation of the momentum equations in order to remove the pressure gradient, the numerical evaluation of third-order derivatives of the stream function at the boundary becomes necessary. The present method, which is based on a stream function-vorticity formulation, obviates the need for this numerically inaccurate and noisy operation. Instead, quasi-linearized forms of the stress boundary conditions are employed in order to determine the variable values at the free surface.

MATHEMATICAL FORMULATION

Consider the steady, incompressible flow of a Newtonian jet as shown schematically in Figure 1(a). Creeping flow is assumed and consequently inertial forces may be neglected. For convenience, velocities are non-dimensionalized by the average velocity, V, the

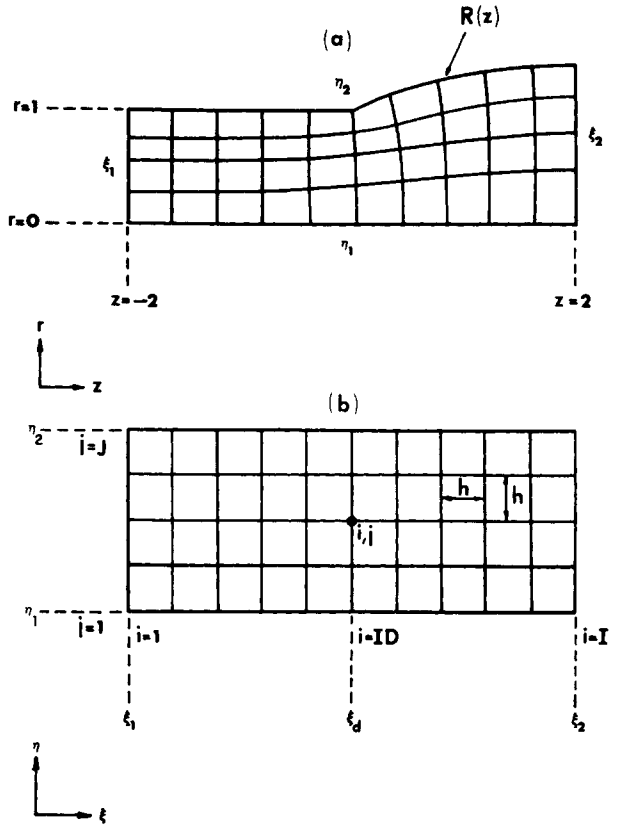

Figure 1. Schematic diagram of the computational field in (a) Physical plane (b) transformed plane.

transverse and axial distances by a characteristic length, L_c, and the pressure and stress terms by $\mu V/L_c$. The characteristic length, L_c, is taken to be either the die radius for circular dies or half of the die opening for slit dies.

Incompressibility implies the existence of a stream function, ψ, defined as

$$u = -\frac{1}{r^\alpha}\frac{\partial \psi}{\partial z}, \quad v = \frac{1}{r^\alpha}\frac{\partial \psi}{\partial r} \tag{1}$$

where the geometry indicator, α, is equal to 0 or 1 depending on whether the geometry considered is planar or cylindrical in nature. Note that Eq. 1 identically satisfies the continuity equation given as

$$D = \frac{\partial v}{\partial z} + \frac{1}{r^\alpha}\frac{\partial}{\partial r}(r^\alpha u) = 0 \tag{2}$$

If the vorticity, ω, is defined as

$$\omega = \frac{\partial u}{\partial z} - \frac{\partial v}{\partial r} \tag{3}$$

then the stream function equation is expressed as follows

$$\frac{\partial^2 \psi}{\partial z^2} + \frac{\partial^2 \psi}{\partial r^2} - \frac{\alpha}{r}\frac{\partial \psi}{\partial r} = -r^\alpha \omega \tag{4}$$

After eliminating pressure from the equations of motion, the vorticity transport equation is given by

$$\frac{\partial^2 \omega}{\partial z^2} + \frac{\partial^2 \omega}{\partial r^2} + \frac{\alpha}{r}\frac{\partial \omega}{\partial r} - \frac{\alpha \omega}{r^2} = 0 \tag{5}$$

In addition, the pressure gradients are related to the vorticity by means of the following relationships

$$\frac{\partial p}{\partial z} = G - \frac{1}{r^\alpha}\frac{\partial}{\partial r}(r^\alpha \omega), \quad \frac{\partial p}{\partial r} = \frac{\partial \omega}{\partial z}$$

where the gravity parameter, $G = \rho g L_c^2/\mu V$, is a measure of the relative importance of the gravitational to the viscous forces.

The appropriate boundary conditions for the present flow problem are formulated as follows:

(i) At a distance very far upstream from the die exit the flow is that of fully developed Poiseuille flow, thus

$$\text{at } z = -\infty,\ 0 \le r \le 1,\ \psi = \frac{1}{2}\left(\frac{3+\alpha}{1+\alpha} r^{1+\alpha} - r^{\alpha+3}\right), \quad \omega = (3+\alpha)r \tag{6a}$$

(ii) At a distance very far downstream from the die exit, the velocity is uniform over the entire cross-section. Therefore

$$\text{at } z = \infty,\ 0 \le r \le R(\infty),\ \psi = \frac{1}{\alpha+1}\left[\frac{r}{R(\infty)}\right]^{\alpha+1},\ \omega = 0 \tag{6b}$$

where $R(z)$ describes the shape of the jet surface.

(iii) At the centerline, symmetry considerations imply

$$\text{at } r = 0,\ -\infty \le z \le \infty,\ \psi = 0,\ \omega = 0 \tag{6c}$$

(iv) the remaining boundary involves mixed boundary conditions since a portion of the boundary comprises a no-slip wall, whereas the rest of the boundary constitutes a free surface. If the die exit is assumed to be located a $z = 0$, then

(a) Within the die, the no-slip condition applies and therefore

$$\text{at } r = 1,\ -\infty \le z \le 0,\ \psi = \frac{1}{\alpha+1},\ \omega = -\frac{\partial^2 \psi}{\partial r^2} = -\frac{\partial v}{\partial r} \tag{6d}$$

(b) At the free surface the stress component tangential to the free surface must vanish. Thus

$$\text{at } r = R(z),\ 0 < z \le \infty,$$

$$T_t = \left[\left(1 - \left(\frac{dR}{dz}\right)^2\right)T_{rz} + \frac{dR}{dz}(T_{rr} - T_{zz})\right] \Big/ \left[1 + \left(\frac{dR}{dz}\right)^2\right] \tag{6e}$$

Also, the normal stress component must be balanced by the tractions due to surface tension forces and the pressure exerted on the surface by the surrounding medium. Therefore

$$T_N = \left[T_{rr} + \left(\frac{dR}{dz}\right)^2 T_{zz} - 2\frac{dR}{dz}T_{rz}\right] \Big/ \left[1 + \left(\frac{dR}{dz}\right)^2\right] = -P_a + HS \tag{6f}$$

where the total curvature of the jet surface, H, is given as

$$H = \frac{\dfrac{d^2R}{dz^2}}{\left[1 + \left(\dfrac{dR}{dz}\right)^2\right]^{3/2}} - \frac{\alpha}{R\left[1 + \left(\dfrac{dR}{dz}\right)^2\right]^{1/2}} \tag{6g}$$

and T_{mn} is the total stress defined as

$$T_{mn} = -p\delta_{mn} + \left(\frac{\partial v_m}{\partial x_n} + \frac{\partial v_n}{\partial x_m}\right) \tag{6h}$$

and $S = \sigma/\mu V$ is the surface tension parameter. Since the free surface represents a streamline, $\psi = 1/(\alpha+1)$, the surface gradient, dR/dz, is therefore related to the surface velocity components by the kinematic condition

$$\frac{dR}{dz} = -\frac{\partial \psi/\partial z}{\partial \psi/\partial r} = \frac{u}{v} \tag{6i}$$

The problem thus entails simultaneous solution of Eqs. 3 and 4 subject to the boundary conditions given by Eq. 6. However, before proceeding with the numerical solution of the governing equations, the irregular flow domain is transformed into a rectangular region by means of a conformal transformation.

COORDINATE TRANSFORMATION

Figure 1 schematically represents the computational field in both the physical and the transformed plane. It is seen that the irregularly-shaped flow domain in the physical (r,z) plane is mapped into

a uniform rectangular region in the transformed (η,ξ) plane. This transformed domain, where $\xi_1 \le \xi \le \xi_2$ and $\eta_1 \le \eta \le \eta_2$, is chosen to be the computational field since the curved free surface is now coincident with the η_2 boundary, thereby permitting the free-surface conditions to be enforced directly and accurately at the boundary. For simplicity, the transformed coordinates η and ξ are chosen to be mutually orthogonal. For this transformation to be valid, it can be shown that the following conditions apply (Thom and Apelt, 1961; Thompson et al., 1977)

$$A = z_\xi = r_\eta = C\eta_r = C\xi_z \tag{7}$$

$$B = r_\xi = -z_\eta = -C\eta_z = C\xi_r \tag{8}$$

$$z_{\xi\xi} + z_{\eta\eta} = 0 \tag{9}$$

$$r_{\xi\xi} + r_{\eta\eta} = 0 \tag{10}$$

where

$$C = A^2 + B^2. \tag{11}$$

Using Eqs. 7, 8, and 11, the governing Eqs. 4 and 5 can be written as (Thompson et al., 1977)

$$\psi_{\xi\xi} + \psi_{\eta\eta} - \frac{\alpha}{r}(A\psi_\eta + B\psi_\xi) = -r^\alpha C\omega \tag{12}$$

and

$$\omega_{\xi\xi} + \omega_{\eta\eta} + \frac{\alpha}{r}(A\omega_\eta - B\omega_\xi) - \frac{\alpha\omega C}{r^2} = 0 \tag{13}$$

In addition, the velocities, the continuity equation, and the vorticity are given as follows

$$v = \frac{1}{Cr^\alpha}(A\psi_\eta + B\psi_\xi),\ u = \frac{1}{Cr^\alpha}(B\psi_\eta - A\psi_\xi) \tag{14}$$

$$D = \frac{\alpha u}{r} + \frac{1}{C}(Au_\eta + Bu_\xi + Av_\xi - Bv_\eta) = 0 \tag{15}$$

$$\omega = \frac{1}{C}(Au_\xi - Bu_\eta - Av_\eta - Bv_\xi) \tag{16}$$

Also, the pressure gradients are related to the vorticity by means of the following expressions

$$p_\xi = AG - \frac{\alpha\omega A}{r} - \omega_\eta \tag{17}$$

$$p_\eta = -BG + \frac{\alpha B\omega}{r} + \omega_\xi \tag{18}$$

and the relevant total stress components defined by Eq. 6h, are given by

$$T_{rr} = -p + \frac{2}{C}(Au_\eta + Bu_\xi) \tag{19a}$$

$$T_{zz} = -p + \frac{2}{C}(Av_\xi - Bv_\eta) \tag{19b}$$

$$T_{rz} = \frac{1}{C}(Au_\xi - Bu_\eta + Av_\eta + Bv_\xi) \tag{19c}$$

The numerical solution now involves the simultaneous solution of four equations, namely, Eqs. 9, 10, 12, and 13. Thus, the transformation procedure has increased the number of equations that is to be solved. In other words, the original problem that was formulated with relatively simple governing equations and complex boundary conditions has been transformed to a problem involving a somewhat more complex system of equations but simpler boundary conditions. In terms of the transformed coordinates the boundary conditions are prescribed as follows:

(i) at $\xi = \xi_1,\ \eta_1 \le \eta \le \eta_2$

$$z = -L_1,\ r_\xi = 0,\ \psi = \frac{1}{2}\left(\frac{\alpha+1}{\alpha+3}r^{\alpha+1} - r^{\alpha+3}\right),\quad \omega = (\alpha+3)r \tag{20}$$

(ii) at $\xi = \xi_2,\ \eta_1 \le \eta \le \eta_2$

$$z = L_2,\ r_\xi = 0,\ \psi = \frac{1}{\alpha+1}\left[\frac{r}{R(L_2)}\right]^{\alpha+1},\ \omega = 0 \tag{21}$$

(iii) at $\eta = \eta_1,\ \xi_1 \le \xi \le \xi_2$

$$r = 0,\ z_\eta = 0,\ \psi = 0,\ \omega = 0 \tag{22}$$

At the boundary $\eta = \eta_2$, the region $\xi_1 \le \xi \le \xi_d$ represents the die wall, Figure 1(b). The no-slip condition therefore gives

(iv) at $\eta = \eta_2,\ \xi_1 \le \xi \le \xi_d$

$$r = 1,\ z_\eta = 0,\ \psi = \frac{1}{\alpha+1},\ \omega = -\frac{\psi_{\eta\eta}}{rA^2} = -\frac{v_\eta}{A} \tag{23}$$

(v) At the free surface, that is at $\eta = \eta_2,\ \xi_d < \xi \le \xi_2$

$$\psi = \frac{1}{\alpha+1} \tag{24}$$

which implies that

$$\frac{dR}{dz} = \frac{u}{v} = B/A \tag{25}$$

Therefore from Eqs. 7 and 8 one obtains

$$r_\xi = \frac{u}{v}z_\xi \tag{26}$$

and

$$z_\eta = -\frac{u}{v}r_\eta \tag{27}$$

Moreover, making use of Eqs. 19 and 25, the tangential and normal stress conditions at the free surface can be expressed as follows

$$v_\eta = \frac{B}{A}(v_\xi - u_\eta) - u_\xi \tag{28}$$

$$u_\eta = \frac{C}{2A}(p_a - p) + \frac{B}{A}v_\eta + \frac{C}{2A}SH \tag{29}$$

The salient features of the numerical technique devised to solve the boundary-value problem represented by Eqs. 20 to 29 are described in the following section. It should be noted that the orthogonality of the curvilinear coordinates is not a requirement of the present approach, but rather a convenient simplification. For situations where orthogonality may not be desirable, a more general and powerful technique for generating "body-fitted curvilinear coordinate systems" has been developed by Thompson et al. (1974, 1977).

NUMERICAL TECHNIQUE

Ideally, the boundary conditions represented by Eqs. 20 and 21 are valid at distances infinitely far from the exit plane. However, prior finite element calculations and recent experimental investigations by Higashitani et al. (1976), Whipple and Hill (1978), and by Gottlieb and Bird (1979) indicate that the exit region approximately lies within a distance of about half of the die opening both upstream and downstream from the exit plane. As a result, the computational region is restricted to lie within $z = -L_1$ and $z = L_2$, where L_1 and L_2 have been assigned a value of 2 throughout the course of this study. The computational field so chosen is then discretized into an $I \times J$ grid with uniform spatial increment, h; I and J being the number of discrete nodes in the ξ and η direction, respectively.

Each of the governing Eqs. 9, 10, 12, and 13 is expressed in finite difference form with the aid of central difference operators. If ϕ is any arbitrary variable, these equations can be written in general form as follows

$$\phi_{ij} = \left[\frac{1}{4}\Delta\phi_{ij} + Y_{ij} + E_{ij}(A_{ij}(\phi_{i,j+1} - \phi_{i,j-1}) + B_{ij}(\phi_{i+1,j} - \phi_{i-1,j}))\right] \Big/ F_{ij} + 0(h^2) \tag{30}$$

TABLE 1. COEFFICIENTS IN THE FINITE DIFFERENCE EQUATIONS

Variable	Y	E	F
r	0	0	1
z	0	0	1
ω	0	$\frac{h\alpha}{8r}$	$1 + \frac{h^2C\alpha}{4r^2}$
ψ	$\frac{1}{4}h^2rC\omega$	$-\frac{h\alpha}{8r}$	1

where

$$\Delta\phi_{ij} = \phi_{i+1,j} + \phi_{i-1,j} + \phi_{i,j+1} + \phi_{i,j-1}$$

$$A_{ij} = \frac{1}{2h}(r_{i,j+1} - r_{i,j-1}) = \frac{1}{2h}(z_{i+1,j} - z_{i-1,j}) \quad (31)$$

$$B_{ij} = \frac{1}{2h}(z_{i,j-1} - z_{i,j+1}) = \frac{1}{2h}(r_{i+1,j} - r_{i-1,j})$$

$$C_{ij} = A_{ij}^2 + B_{ij}^2$$

The expressions for the coefficients Y, E, and F for each of the variables are summarized in Table 1. Equation 30 is used to compute variable values only for the interior points of the field ($1 < i < I$, $1 < j < J$). At the boundaries, one-sided second-order differencing is employed to evaluate the gradients necessary to enforce the boundary conditions.

Figure 2 illustrates the salient features of the computational procedure adopted for solving the governing finite difference equations. The method of solution, based on an iterative scheme, can be outlined as follows:

1. Initialize variables by supplying an initial guess for the solution.
2. Compute the surface shape from Eq. 25. Numerically, this is expressed as

$$r_{i+1,J}^{(k_1+1)} = r_{i,J}^{(k_1+1)} + \int_{z_{i,J}^{(k_1)}}^{z_{i+1,J}^{(k_1)}} (u/v)^{(k_1)} dz, \quad ID < i \le I \quad (32)$$

where $r_{ID,J} = 1$ and k_N is the iteration level for loop N as shown in Figure 2.

3. Keeping the shape of the surface unchanged, the boundary conditions on r are updated. The r-field is iterated once and overrelaxed by a factor of 1.5.
4. If $|r_{ij}^{(k_2+1)} - r_{ij}^{(k_2)}| > \epsilon_2$, step 3 is repeated.
5. The boundary conditions on z are updated. For $ID < i \le I$,

$$z_{ij}^{(k_3+1)} = \frac{1}{3}\left[4z_{i,J-1}^{(k_3)} - z_{i,J-2}^{(k_3)} - \frac{u_{iJ}}{v_{iJ}}\left(r_{i,J-2} + 3r_{iJ} - 4r_{i,J-1}\right)\right] \quad (33)$$

   The z-field is iterated once and overrelaxed by a factor of 1.5.
6. If $|z_{ij}^{(k_3+1)} - z_{ij}^{(k_3)}| > \epsilon_3$, step 5 is repeated.
7. The generated coordinate system (r,z-field) is allowed to settle by repeating steps 3 to 6 several times, usually five.
8. The vorticity field, ω, is iterated once followed by one iteration on the stream function, ψ. Both variables are underrelaxed by a factor of 0.5.
9. Compute the velocities at interior points from central difference analogs of Eq. 14.
10. Update boundary conditions. Apart from those at the $\eta_2 (j = J)$ boundary, the conditions are relatively straightforward to enforce as they are either Dirichlet or Neumann type. The boundary at $\eta = \eta_2$, however, requires special treatment. Over the no-slip portion of the boundary, the vorticity is obtained from the following expression

$$\omega_{ij}^{(k_5)} = \frac{1}{2hA_{ij}}\left(4v_{i,J-1}^{(k_5)} - v_{i,J-2}^{(k_5)}\right) \text{ for } 1 \le i \le ID \quad (34)$$

At the free surface, where $ID < i \le I$, the calculation scheme is more involved and proceeds in the following order:

(i) First, the surface vorticity is obtained from the equation

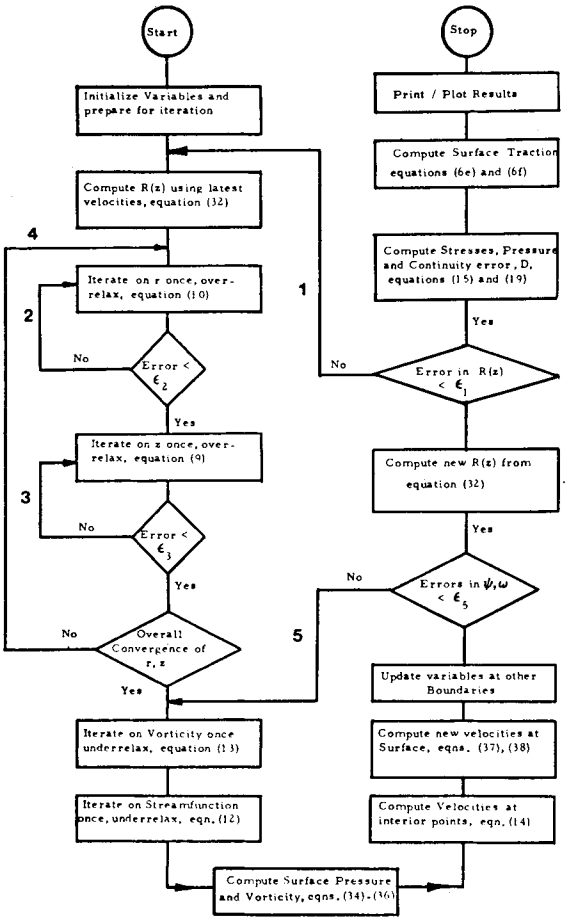

Figure 2. Flow diagram of the computational algorithm.

$$\omega_{ij}^{(k_5+1)} = \left[\frac{A(u_\xi - v_\eta) - B(u_\eta + v_\xi)}{C}\right]_{iJ}^{(k_5)} \quad (35)$$

where $[\ ]_{ij}^{(k_N)}$ denotes evaluation at the grid node (i,j) for the kth iteration in the loop numbered N in Figure 2.

(ii) The surface pressure is then obtained by numerically integrating Eq. 17 along the surface, that is

$$p_{ij}^{(k_5+1)} = p_{i-1,J}^{(k_5+1)} + \int_{z_{i-1}}^{z_i}\left(AG - \frac{\alpha\omega A}{r} - \omega_\eta\right)dz \quad (36)$$

where

$$p_{IJ} = p_a + \alpha S/r_{IJ}$$

(iii) The surface pressure is next used to obtain the surface velocities from the quasi-linearized forms of the free-surface stress conditions. This gives

$$v_{ij}^{(k_5+1)} = \frac{1}{3}\left(4v_{i,J-1}^{(k_5+1)} - v_{i,J-2}^{(k_5+1)} + 2h\left[\frac{B}{A}(v_\xi - u_\eta) - u_\xi\right]_{iJ}^{(k_5)}\right) \quad (37)$$

$$u_{ij}^{(k_5+1)} = \frac{1}{3}\left(4u_{i,J-1}^{(k_5+1)} - u_{i,J-2}^{(k_5+1)} + \frac{hC}{A_{iJ}}(p_{ij}^{(k_5+1)} - p_a) + 2h\left[\frac{B}{A}v_\eta + \frac{CSH}{2A}\right]_{iJ}^{(k_5)}\right) \quad (38)$$

11. If $|\omega_{ij}^{(k_5+1)} - \omega_{ij}^{(k_5)}| > \epsilon_5$ or $|\psi_{ij}^{(k_5+1)} - \psi_{ij}^{(k_5)}| > \epsilon_5$, steps 8 to 10 are repeated.
12. A new surface profile is computed using Eq. 32 with the latest surface velocities.
13. If $|r_{ij}^{(k_1+1)} - r_{ij}^{(k_1)}| > \epsilon_1$, steps 2 to 12 are repeated.
14. Secondary variables such as pressure, stress, and the continuity error, D, are calculated.

TABLE 2. EFFECT OF MESH REFINEMENT ON DIE SWELL AND THE VARIABLES AT THE DIE LIP: S = 0, G = 0

Variables	21 × 6 $h = 0.2$	41 × 11 $h = 0.1$	81 × 21 $h = 0.05$
	Axisymmetric, $\alpha = 1$		
% Swell	12.30	12.00	12.00
p	−0.558	−2.037	−3.977
T_{rz}	−5.337	−8.121	−10.800
T_{zz}	11.330	20.090	33.430
T_{rr}	−1.207	−1.506	−2.087
D	−1.181	−2.040	−3.163
Relative Cost	1.0	6.509	>35.4
	Plane, $\alpha = 0$		
% Swell	17.40	16.10	16.10
p	−0.959	−2.163	−3.792
T_{rz}	−4.906	−7.312	−9.614
T_{zz}	11.850	19.610	31.640
T_{rr}	−0.758	−1.179	−1.831
D	−1.156	−1.897	−2.876
Relative Cost	1.0	8.583	>43.28

15. Hard copy plots and prints of all variables are generated.

The numerical scheme outlined above proved to be very efficient and reasonably simple to code for the Newtonian jet swell problem considered here. In all cases, the acceptable errors in the converged solution were taken to be: $\epsilon_1 = 0.5 \times 10^{-3}$, $\epsilon_2 = \epsilon_3 = \epsilon_5 = 10^{-4}$. The starting values for a given case were taken as the converged solution for the set of parameter values nearest to those under consideration. Initially, however, the "stick-slip" problem (Richardson, 1970 a,b) was solved and this solution was used as the starting point for the die swell case where no gravitational and surface tension effects were present. Apart from the absence of the curved boundary, the flow field in the "stick-slip" problem closely resembles that of the present problem. Moreover, for this model case, all of the boundary conditions discussed previously remain valid except for the condition at the free surface, which becomes (Dutta, 1980)

at $j = J, ID < i \leq I$

$$r = 1, z_\eta = 0, \psi = \frac{1}{\alpha + 1}, \omega = 0 \quad (39)$$

The zero vorticity condition results from the requirement that the surface shear stress must vanish. Clearly, the coordinate transformation is redundant for solving this idealized case.

It should also be mentioned that even though the computational region is restricted to lie within $z = -2$ to $z = +2$, the exit will not coincide exactly with the location $z = 0$ because of the nature of the condition given by Eq. 23. Therefore, once the numerical solution is obtained, the computational region is translated axially by the appropriate amount so that $z_{ID,J} = 0$. This adjustment does not alter the numerical results in any way, but merely facilitates comparison with other numerical predictions. However, it should be noted that this will casue the axial locations of the upstream and downstream boundaries to be slightly different from −2 and +2, respectively. Furthermore, for all of the calculations presented here, the limits on ξ and η are taken to be: $\xi_1 = -2$, $\xi_2 = 2$, $\xi_d = \eta_1 = 0$ and $\eta_2 = 1$. Also, for convenience, the pressure in the surrounding fluid has been chosen as the reference pressure such that $p_a = 0$ for all of the cases considered in the following discussion.

RESULTS AND DISCUSSION

Jet Swell in the Absence of Gravity and Surface Tension

In order to evalute the effectiveness of the numerical scheme, the Newtonian jet swell problem was first solved by neglecting gravitational and surface tension effects. The computations were performed on three different mesh sizes in order to select an optimum grid for further calculations. The results are presented in Table 2. As the grid size is reduced from a coarse to an intermediate mesh, the die swell decreases. However, beyond this mesh size the extent of swell remains unaffected by any change in the grid structure. The corresponding computational cost increases substantially as the number of discrete mesh points increases. Thus, all calculations reported subsequently were performed using a 41 × 11 grid. In general, the numerical procedure proved to be very efficient in solving the die swell problem. For example, the axisymmetric case required about 5 minutes of CPU time on a Cyber CDC 174 machine as compared to about 20 minutes required by the finite element scheme of Nickell et al. (1974) on an IBM 360/67 computer. Furthermore, the die exit, where the liquid separates from the solid boundary of the die, involves severe stress singularities (Michael, 1958; Huilgol and Tanner, 1977; Sturges, 1979). This occurs because of the different nature of the boundary conditions on the upstream and downstream side of the die exit. The results in Table 2 clearly demonstrate this behavior. Irrespective of the mesh size, the results indicate a sudden transition from a very high shear stress to an even larger axial stress. Ideally, as $h \to 0$, the stresses at the die lip should be infinite, and the numerical predictions indeed tend to exhibit this singular behavior.

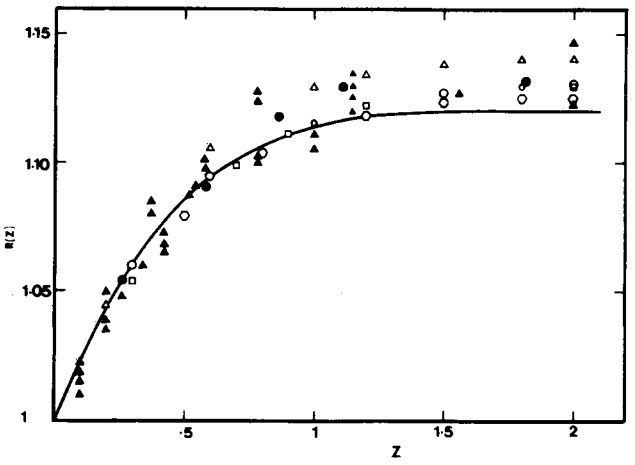

Figure 3. Comparison between numerical and experimental surface profiles for axisymmetric jets, $S = 0$, $G = 0$. Numerical: — Present work; ○ Nickell et al. (1974); △ Chang et al. (1979); Galerkin, 3 × 9 elements; □ Omodei (1980); ○ Crochet et al. (1980). Experimental: ▲ Batchelor et al. (1973), Parlac, Re ≈ 10^{-8}; ● Nickell et al., Silicone, Re < 10^{-3}.

Figure 3 shows the surface profile of a creeping Newtonian jet issuing from a circular die. The numerial results have been compared with the experimental measurements of Batchelor et al. (1973) and Nickell et al. (1974) along with the results obtained from different finite element schemes. As can be seen, a die swell value of 12% as predicted by the present finite difference method is in

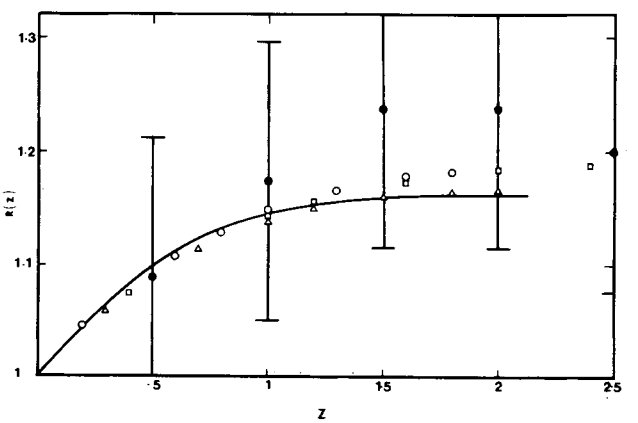

Figure 4. Comparison between numerical and experimental surface shapes for plane jets, $S = 0$, $G = 0$. Numerical: — Present work; △ Chang et al. (1979); Collocation, 3 × 10 elements; ○ Omodei (1979); □ Crochet et al. (1980). Experimental: ● Whipple and Hill (1978), Silicone, Re = 3.5 × 10^{-4}. Error bars are for ± one standard deviation.

reasonably close agreement with the available experimental observations and numerical predictions. The surface profile for a plane jet is illustrated in Figure 4. In this case, the agreement between the numerical predictions and the experimental data can at best be judged as fair. However, it should be noted that the experimental die swell has indirectly been obtained from the velocity profile measurements of Whipple and Hill (1978). In order for the mass to be conserved in plane jet flow, the die swell ratio should be equal to the ratio of the average velocities at the upstream and downstream boundaries. Hence, as has been indicated by Chang et al. (1979), the experimental die swell, since it is obtained from the ratio of two quantities (average velocities) with large experi-

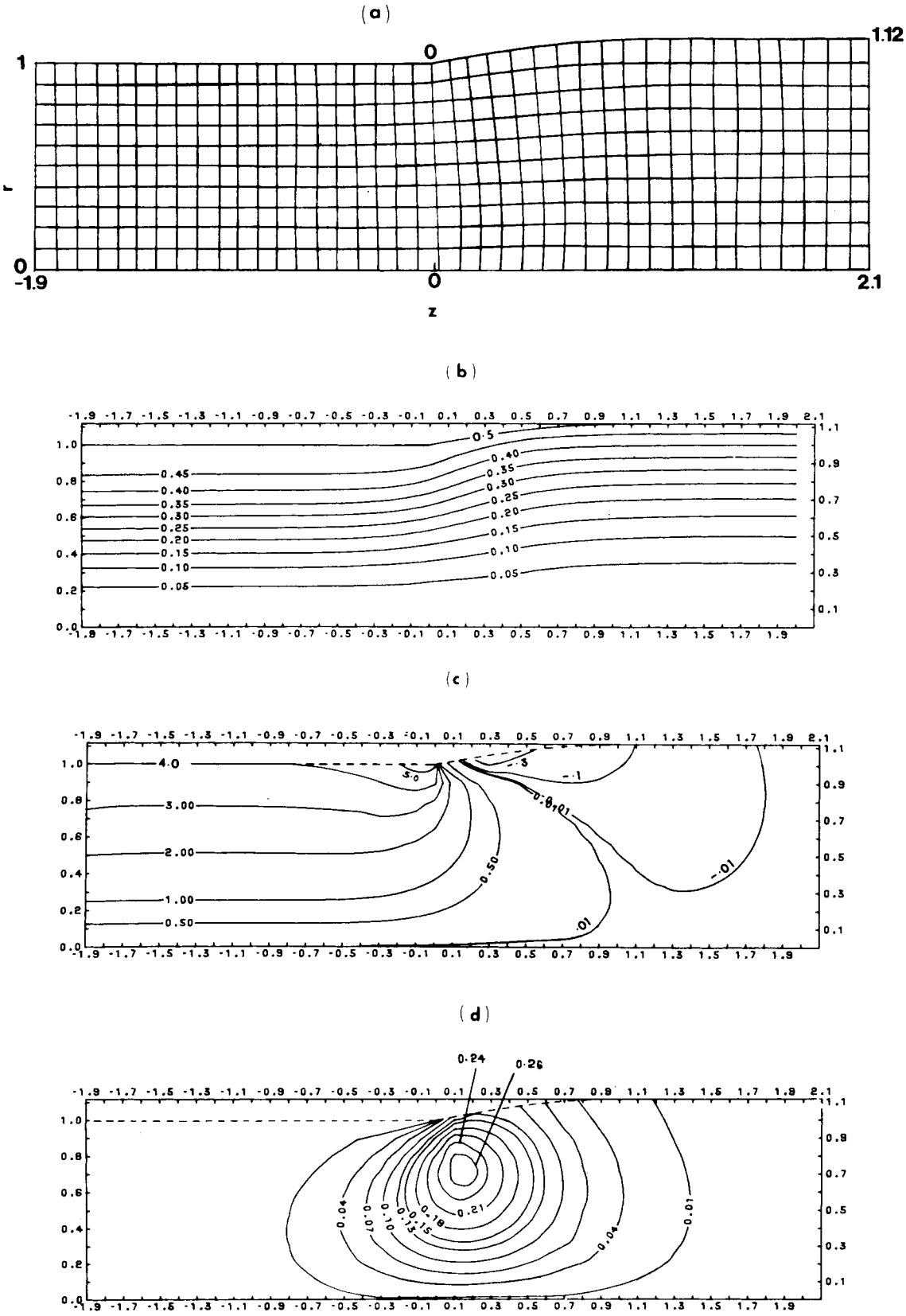

Figure 5. Contour plots for different flow variables in axisymmetric case, $S = 0$ $G = 0$, (a) ξ and η, indicating the grid pattern in the Physical Plane (b) Stream Function (c) Vorticity (d) Radial Velocity (e) Axial Velocity (f) Pressure (g) Total Radial Stress (h) Total Axial Stress (i) Shear Stress.

Fig. 5 (*continued*)

(e)

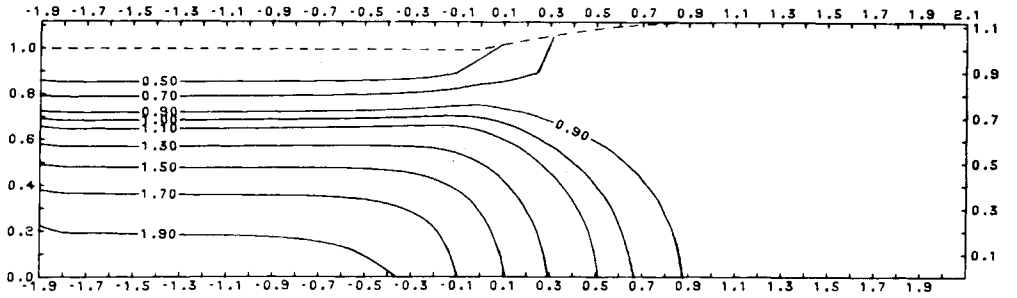

(f)

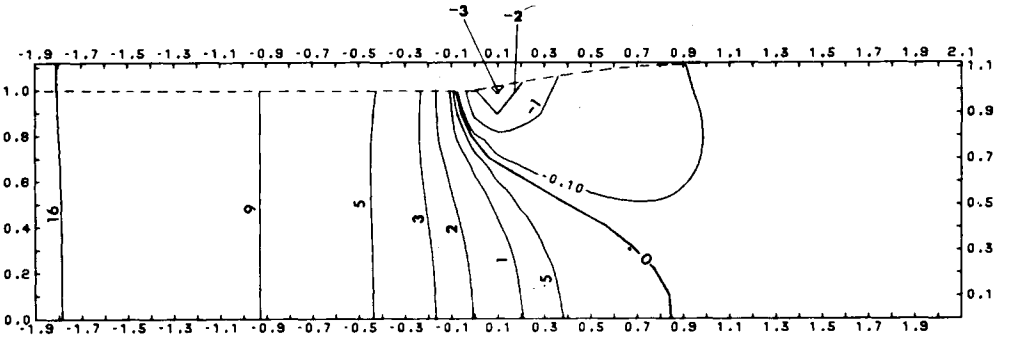

(g)

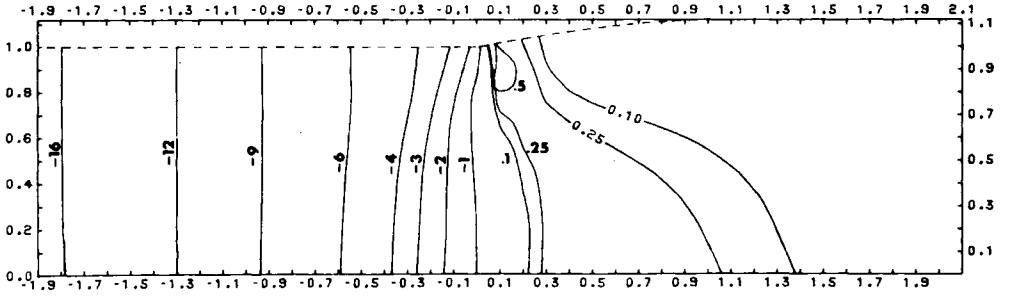

(h)

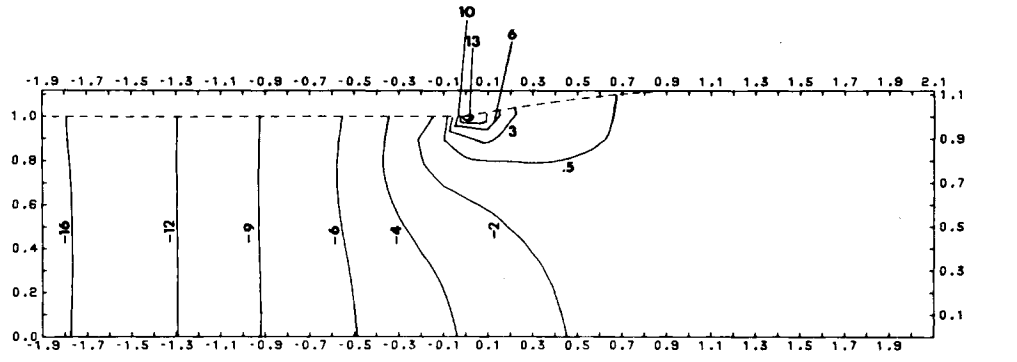

(i)

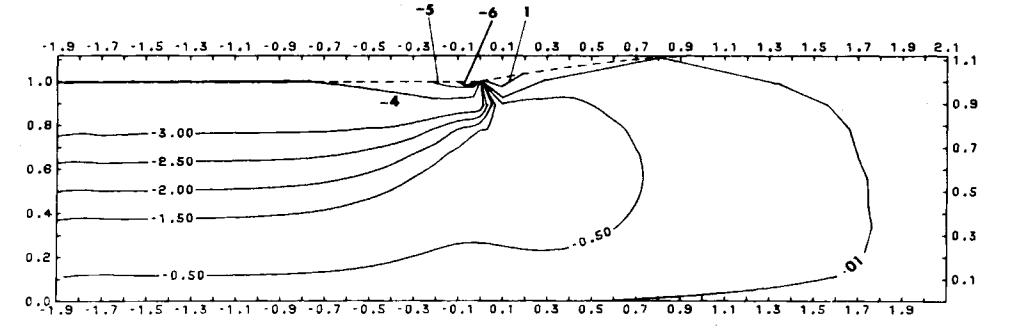

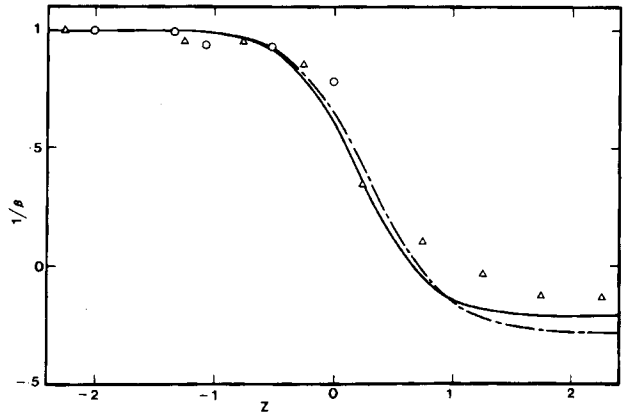

Figure 6. Comparison of velocity profile rearrangement with experimental data. Numerical Solution: — Axisymmetric, -·- Plane. Experimental: ● Gottlieb and Bird (1979), Circular Die, Glycerol, Re = 2.47 × 10^{-2}; ▲ Whipple and Hill (1978), Slit Die, Silicone, Re = 3.5 × 10^{-4}.

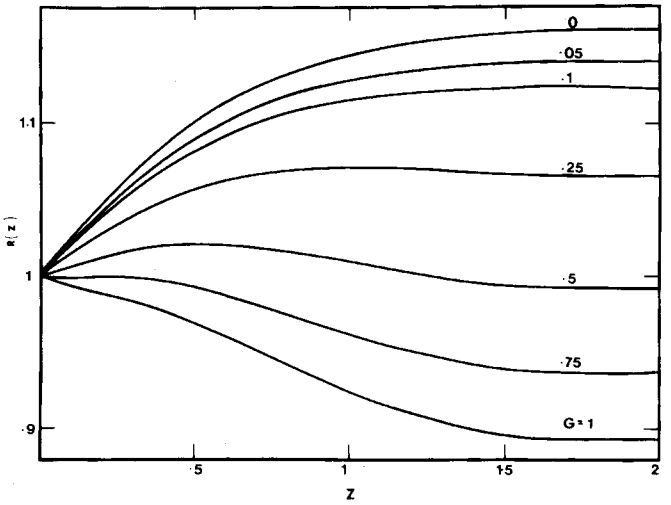

Figure 8. Influence of gravity on the surface profile of a plane jet, $S = 0$.

mental error, is likely to involve a considerable amount of uncertainty. Nevertheless, encouraging qualitative agreement can be observed between the two results.

The remarkable feature of the die swell problem is the rapid flow rearrangement that occurs within a small region both upstream and downstream from the exit. This complex flow behavior can be better appreciated by considering the contour plots of the relevant kinematic and dynamic variables as illustrated in Figure 5(a) to (i) for the case of an axisymmetric jet. Figure 5(a) shows the contours of ξ and η, thereby giving the actual mesh pattern in the physical plane. It is clear that the exit region, within which flow rearrangement occurs from Poiseuille to uniform plug flow, extends approximately from $z = -1$ to $z = 1.5$. Also Figures 5(b) to (e) clearly indicate that the flow is not fully developed at the die exit, primarily because of the absence of inertial forces which allows the vorticity generated at the die lip to diffuse both downstream and upstream from the exit plane. Moreover, as can be seen from Figures 5(g) to (i) the stress field, particularly around the die lip, is extremely complex and highly nonviscometric. Clearly, swelling of the jet is a result of the large normal stresses generated just beyond the exit section. For a plane jet, the qualitative aspects of the flow field were found to be almost identical to that for the axisymmetric case, and hence, will not be discussed in detail here.

A more stringent test of the validity of the numerical solution can be made by comparing the calculated and experimentally measured velocity profile data. Velocity profile measurements within the exit region of creeping Newtonian (and viscoelastic) jet flows have recently been reported by Whipple and Hill (1978) and by Gottlieb and Bird (1979) for slit and circular dies, respectively. The latter study, however, deals only with the exit region inside the die. In both investigations, the axial velocity profiles were fitted to an empirical equation of the form

$$v(r,z) = C_1(z) + C_2(z)[1 - r^{C_3(z)}] \tag{40}$$

where $C_1(z) = 0$ for $z \leq 0$. Mass conservation then implies that

$$C_1 + C_2 - \frac{R^{C_3} C_2(\alpha + 1)}{C_3 + \alpha + 1} - \frac{1}{R^{\alpha} + 1} = 0 \tag{41}$$

where $R(z) = 1$ for $z \leq 0$. Gottlieb and Bird (1979) have defined a relative measure of velocity profile rearrangement as follows

$$\text{for } z \leq 0,\ \beta(z) = \frac{C_3(z)}{C_3(-\infty)} \tag{42}$$

An alternative form for expressing the velocity profile rearrangement is the following:

$$\beta(z) = \frac{C_2(-\infty) - 1}{C_2(z) - 1} \tag{43}$$

The difference between the definitions of β given by Eqs. 42 and 43 is that the former is based on the exponent function, $C_3(z)$, whereas the latter is based on the difference between the maximum and average velocities. In the present study, in order to quantify the relative amount of velocity rearrangement within the entire exit region, the latter definition has been chosen. That is

$$\text{for } -\infty \leq z \leq \infty,\quad \beta(z) = \frac{v(0,-\infty) - 1}{v(0,z) - 1} \tag{44}$$

Note that as $v(0,z) \to 1$, $\beta \to \infty$. Figure 6 shows the variation of $1/\beta$ with axial distance, z. Also shown are the experimental data of Whipple and Hill (1978) and Gottlieb and Bird (1979). Here again, the numerical predictions are in reasonably good agreement with experimentally measured values.

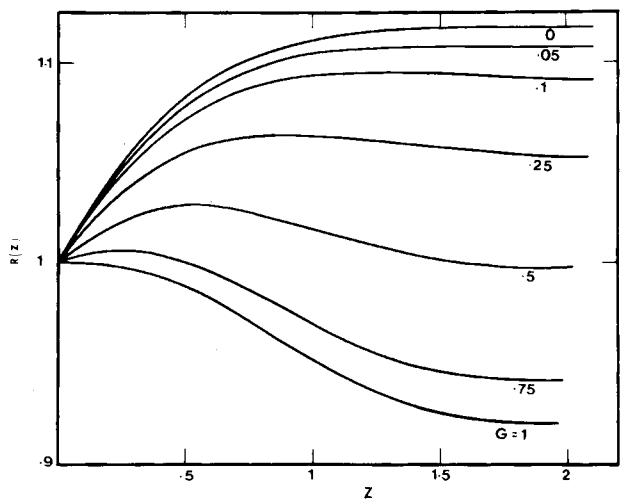

Figure 7. Effect of gravity on the shape of an axisymmetric jet, $S = 0$.

Effect of Gravity

The influence of a gravitational field in determining the final shape of a creeping Newtonian jet is now considered. Certainly, the overall length of the jet is an important factor for this case as has been demonstrated by the recent finite element calculations of Fischer et al. (1980). In the present work, however, only the effect of the gravitational parameter, G, is investigated. The influence of G on surface shape is illustrated in Figures 7 and 8 for the case of an axisymmetric and plane jet, respectively. It is obvious that the final shape of the jet is a result of a dynamic balance between the competing influences of viscous and gravitational forces. For small values of G, the jet swell is less than the gravity-free case, and the radius (or thickness) increases monotonically with axial

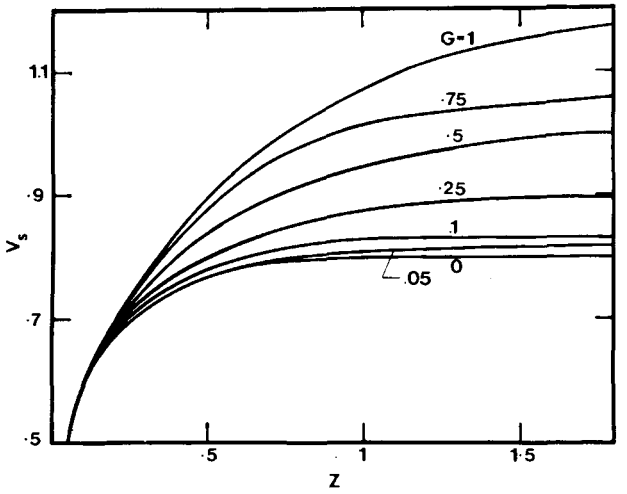

Figure 9. Variation of surface axial velocity with axial distance for different values of G, $S = 0$, axisymmetric case.

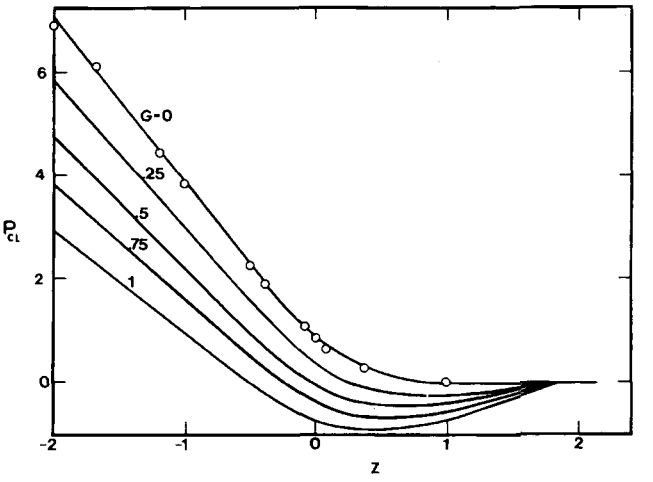

Figure 11. Influence of gravity on the centerline pressure of a plane jet, $S = 0$, O Chang et al. (1979), Collocation, 3 × 10 elements, $G = 0$.

distance. As the magnitude of G is increased, a maximum appears in the surface profile along with a rapid decrease in die swell. Finally, for even larger values of G, the gravitational forces completely dominate the viscous effects and the jet contracts.

The qualitative nature of the flow behavior was determined to be practically independent of the geometry considered. Therefore, no specific reference to the particular geometry is made in the subsequent discussion. Figures 9 and 10 show the axial and transverse velocities along the jet surface for different magnitudes of G. The results clearly demonstrate the discontinuity in the velocity gradient at $z = 0$. Also, as expected, the presence of a gravitational field accelerates the fluid thereby increasing the axial velocity and decreasing the transverse velocity. The net result is a decrease in die swell, which is directly related to the velocity ratio, u/v, at the surface.

Figures 11 and 12 illustrate the variation of the centerline and surface pressures with axial distance. Far upstream from the exit, the pressure is uniform over the cross-section and varies linearly with z due to the Poiseuillean nature of the flow. As the exit section is approached, a transverse pressure gradient begins to develop and continues to do so until the exit plane is traversed. Beyond the exit section, this transverse gradient gradually decays and ultimately the pressure across the jet becomes uniform again. Although the presence of a gravitational field results in an expected decrease in pressure, it does not alter the qualitative nature of the pressure profiles significantly. Moreover, the results in Figure 12 indicate the severe pressure singularity existing at the die lip. This is in accordance with the analytical findings of Michael (1958) and the finite element calculations reported by Chang and coworkers (1979).

Effect of Surface Tension

Surface tension plays an important role in determining the shape of a free surface. Numerical simulations incorporating surface tension, however, involve determination of the curvature of the surface profile. One particular technique, commonly used for curvature calculations, is that based on spline-fitting as has been suggested by Daly (1969), and has been used in a modified form by Omodei (1979, 1980) for the jet swell problem. In the present study, a technique similar to that employed by Reddy and Tanner

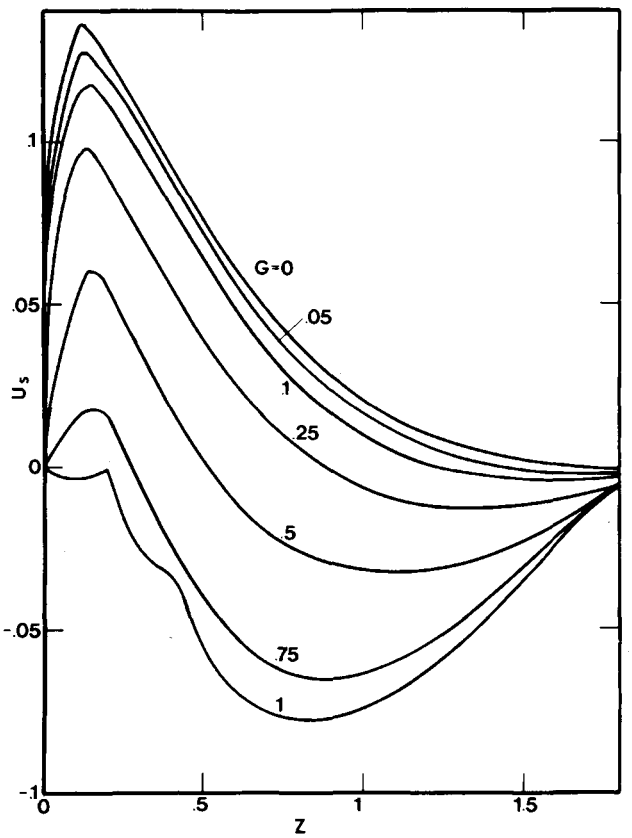

Figure 10. Effect of gravity on surface radial velocity for an axisymmetric jet, $S = 0$.

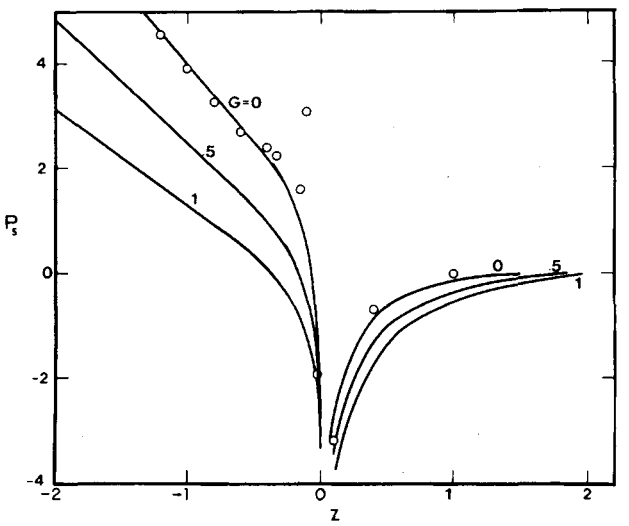

Figure 12. Surface pressure profiles of a plane jet for different values of G, $S = 0$. O Chang et al. (1979), Collocation, 3 × 10 elements, $G = 0$.

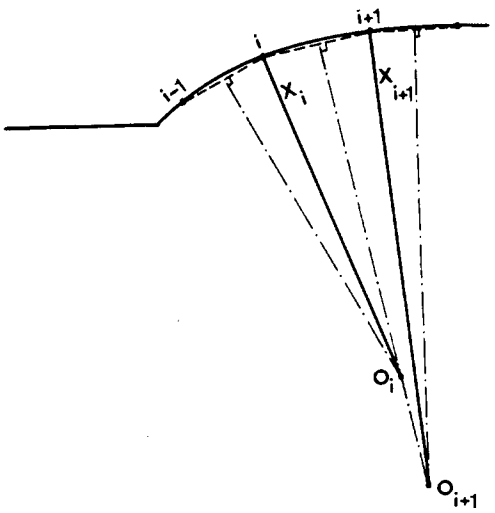

Figure 13. Calculation of the radius of curvature at discrete points on the free surface.

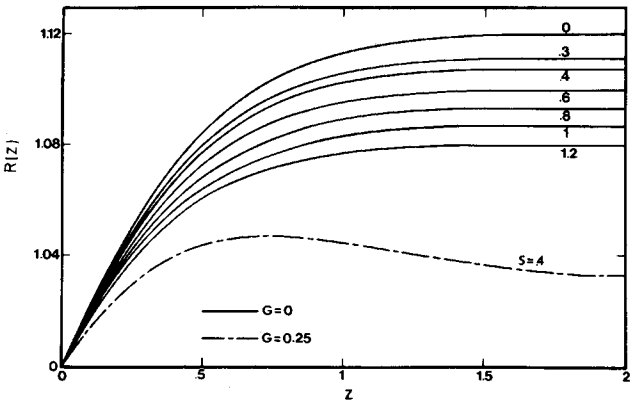

Figure 14. Effect of surface tension on the surface profile of an axisymmetric jet.

(1978a) is adopted. The method determines the radius of curvature, X, of the surface profile by means of a purely geometrical procedure as shown schematically in Figure 13. Once X_i is evaluated at a point i on the free surface, the total curvature at that point is given by

$$H_i = -\left[\frac{1}{X_i} + \frac{\alpha}{R(z_i)(1 + (u_i/v_i)^2)^{1/2}}\right] \tag{45}$$

The curvature, H_i, is then used in Eq. 38 to update the surface variables at point i for every iteration of the stream function-vorticity loop (number 5 in Figure 2).

Figure 14 shows the effect of surface tension on the shape of an axisymmetric jet for different values of the surface tension parameter, S, which measures the ratio of surface tension to viscous forces. Clearly, surface tension inhibits the swelling effect due to the inherent inward normal force on the free surface. Also shown in Figure 14 is a surface profile incorporating both gravitational and surface tension effects. Evidently, the contribution due to gravity in reducing die swell is significantly greater than that owing to surface tension. Qualitatively similar behavior was also obtained regarding the influence of surface tension on the free-surface profile for plane jets (Table 3) and therefore is not discussed here in detail. Instead, the numerical results for a large variety of flow conditions are summarized in Table 3. The dynamic variables at the centerline and at the surface are given at the exit plane along with the corresponding die swell values and exit losses. The exit loss, e, is determined as $e = p_{ex}/2\tau_w$ where p_{ex} is the surface pressure at the exit extrapolated from far upstream, and τ_w is the wall shear stress in Poiseuille flow. It is seen that the singularity at the die lip is most severe when both gravitational and surface tension effects are absent. For the general case, the additional forces which arise due to gravity and surface tension tend to accelerate the fluid thereby reducing the velocity gradients at the die lip, which consequently tend to relieve the pressure and stress singularities.

Also, the die swell values listed in Table 3 for various flow conditions are found to be in reasonably close agreement with both experimentally determined results and with numerical predictions given by various finite element techniques previously reported in

TABLE 3. SUMMARY OF NUMERICAL RESULTS FOR DIFFERENT FLOW CONDITIONS

			at (0, 0)			at (1, 0)			
G	S	% Swell	v	p	e	$-p$	$-T_{rz}$	$-T_{rr}$	T_{zz}
Axisymmetric Jet, $\alpha = 1$									
0.00	0.0	12.00	1.600	2.061	0.214	2.037	8.121	1.506	20.09
0.05	0.0	10.70	1.601	1.686	0.186	2.156	7.358	1.367	20.18
0.10	0.0	9.20	1.602	1.587	0.170	2.209	7.322	1.261	19.60
0.25	0.0	5.30	1.608	1.307	0.128	2.352	7.232	0.973	18.23
0.50	0.0	−0.25	1.611	0.919	0.064	2.587	7.095	0.471	16.40
0.75	0.0	−5.83	1.634	0.745	0.052	2.828	6.969	0.109	14.72
1.00	0.0	−7.90	1.644	0.302	−0.035	2.993	6.843	0.443	14.08
0.00	0.3	11.10	1.611	2.305	0.274	1.765	8.088	1.762	19.59
0.00	0.4	10.70	1.611	2.394	0.246	1.671	8.067	1.844	19.34
0.00	0.6	10.00	1.611	2.578	0.269	1.472	8.017	2.012	18.79
0.00	0.8	9.30	1.612	2.765	0.289	1.266	7.956	2.181	18.21
0.00	1.0	8.60	1.613	2.958	0.309	1.060	7.901	2.354	17.66
0.00	1.2	8.00	1.614	3.154	0.329	0.850	7.843	2.528	17.12
0.25	0.4	3.30	1.617	1.923	0.153	1.952	7.624	1.283	16.89
Plane Jet, $\alpha = 0$									
0.00	0.0	16.10	1.310	0.938	0.169	2.163	7.312	1.179	19.61
0.05	0.0	14.10	1.310	0.721	0.136	2.253	6.552	1.051	19.46
0.10	0.0	12.30	1.311	0.617	0.120	2.311	6.513	0.938	18.75
0.25	0.0	6.60	1.314	0.353	0.066	2.492	6.373	0.594	16.77
0.50	0.0	−0.77	1.321	−0.075	−0.012	2.747	6.138	−0.096	14.42
0.75	0.0	−6.20	1.334	−0.398	−0.077	2.973	5.929	−0.678	12.84
1.00	0.0	−10.50	1.341	−0.735	−0.101	3.179	5.742	−1.208	11.69
0.00	0.5	14.00	1.310	0.896	0.158	2.171	6.575	1.109	19.52
0.00	0.75	13.10	1.310	0.893	0.160	2.152	6.556	1.094	19.09
0.00	1.00	10.30	1.312	0.929	0.139	2.131	6.470	0.980	17.74
0.00	2.00	9.20	1.313	0.904	0.154	2.056	6.425	1.015	17.03
0.25	0.50	5.60	1.316	0.416	0.064	2.465	6.345	0.502	16.36

TABLE 4. NORMAL AND TANGENTIAL STRESSES ON THE JET SURFACE

Z	$T_t \times 10^3$	$T_N \times 10^3$	D
	$S = 0, G = 0, \alpha = 1$		
0.0718	1.715	3.586	5.425
0.1634	1.004	4.995	2.776
0.2643	0.564	5.067	2.251
0.5864	0.076	2.079	1.076
1.0250	0.000	0.315	0.309
1.5670	0.000	−0.042	0.019
	$S = 0, G = 0.5, \alpha = 1$		
0.0904	0.404	1.051	4.441
0.1902	−0.299	0.724	1.909
0.2957	−0.291	0.207	1.372
0.6152	−0.093	−0.470	0.252
1.0300	0.183	−0.384	−0.328
1.5300	0.354	−0.124	−0.277
	$S = 0, G = 0, \alpha = 0$		
0.0676	1.827	0.026	5.141
0.1557	0.990	1.453	2.853
0.2537	0.700	1.935	2.471
0.5729	0.101	1.635	1.481
1.0200	−0.275	0.652	0.611
1.5810	−0.238	0.050	0.107

Z	$T_t \times 10^3$	T_N	D	$(T_N)_{appl}$
	$S = 1.0, G = 0, \alpha = 1$			
0.0776	−2.572	−1.129	5.054	−1.128
0.1734	−0.515	−1.237	2.380	−1.234
0.2766	−0.421	−1.256	1.857	−1.253
0.5955	0.335	−1.074	0.881	−1.071
1.0260	0.264	−0.975	0.246	−0.975
1.5600	−0.059	−0.932	0.012	−0.933
	$S = 0.5, G = 0, \alpha = 0$			
0.0702	−2.121	−0.0351	5.101	−0.0357
0.1610	−0.845	−0.1112	2.647	−0.1097
0.2607	−0.532	−0.1530	2.250	−0.1506
0.5792	0.165	−0.0932	1.348	−0.0909
1.0220	0.187	−0.0496	0.544	−0.0487
1.5770	0.023	−0.0161	0.090	−0.0159
	$S = 0.5, G = 0.25, \alpha = 0$			
0.0833	−0.512	−0.0286	4.434	−0.0273
0.1801	−0.493	−0.0999	2.074	−0.0973
0.2834	−0.404	−0.1362	1.661	−0.1330
0.6009	−0.088	−0.0670	0.795	−0.0639
1.0260	0.058	−0.0225	0.156	−0.0206
1.5480	0.037	−0.0053	0.035	−0.0051

the literature (Omodei, 1979, 1980; Reddy and Tanner, 1978a, 1978b).

Boundary Conditions

The extent to which the pressure and stress boundary conditions are satisfied is now briefly discussed. At the upstream boundary, Poiseuille flow has been assumed, and therefore the pressure should remain uniform across the entire cross-section. From the numerical results, it is found that the maximum deviation of pressure from its average value is less than 1%. At the downstream boundary,

$$T_{zz} = -p = -\alpha S/[R(L_2)],$$

which implies that the axial velocity gradient, $\partial v/\partial z$, must vanish. The axial velocity gradients, calculated from the numerical results, vary from 0 to 10^{-3} over the entire cross-section. Thus, within acceptable numerical error, both the up-stream and downstream conditions are satisfied adequately.

Ideally, the continuity equation given by Eq. 2 and the stress conditions represented by Eqs. 6e and 6f are to be satisfied at the free surface. In general, numerical solutions have not been successful in meeting all of these requirements simultaneously, especially near the die lip. In the case of finite element calculations, where the continuity equation is solved directly, Chang et al. (1979) and Omodei (1979, 1980) have reported that both normal and tangential stresses on the surface differed significantly from their expected values. Similar observations can also be noticed from the finite difference result of Horsfall (1973). This discrepancy, however, decays almost exponentially as one moves downstream from the exit.

Contrary to the numerical methods mentioned above, the present procedure does not solve the continuity equation explicitly. Instead, mass conservation is ensured by using a stream function approach and the velocities are obtained everywhere in the field, except at the free surface, from the stream function derivatives. Velocities at the free surface are determined from the stress conditions. Table 4 summarizes the surface stresses and the error in the continuity equation, D, for the different cases of creeping jet flow considered. Also listed is the imposed normal stress, $(T_N)_{appl} = HS$. Note that when surface tension is ignored, the imposed normal stress is zero at the free surface. The results demonstrate that both the normal and tangential stress conditions are very well satisifed, but failure occurs in satisfying continuity. Since continuity cannot be satisifed exactly at the die exit because of singularity problems, the present solution scheme chooses to satisfy the stress conditions rigorously, but relaxes the continuity requirement. It appears that at the present state of development, irrespective of whether a finite element or finite difference method is used, the numerical schemes are incapable of satisfying all of the requirements at the free surface simultaneously, particularly in the immediate vicinity of the die lip. Nevertheless, in spite of this disconcerting deficiency, the numerical solutions predict the overall shape and the swell quite accurately as is evident from the good agreement with available experimental results.

CONCLUDING REMARKS

The present work puts forward a simple and efficient finite difference technique for solving steady, viscous free-surface flows. The method has been successfully employed to solve the Newtonian jet swell problem. The transformation procedure employed here permits the present method to achieve the boundary generality of the finite element technique. Consequently, the solution scheme can be applied to a large variety of flow problems involving arbitrarily curved boundaries, which may or may not constitute a free surface.

For the jet swell problem considered here, stress singularities exist at the die exit. Thus, the numerical solution cannot be expected to be very accurate in the neighborhood of the die exit as all boundary conditions cannot be satisfied rigorously. If, however, a more precise solution in the immediate vicinity of the singularity is desired, it may be fruitful to incorporate special numerical techniques (Crank and Furzeland, 1975) for treating boundary singularities into the basic computational scheme presented here.

Notation

A, B, C = transformation parameters
C_1, C_2, C_3 = coefficients in empirical equation for axial velocity
D = error in continuity equation
e = exit loss
E, F = coefficient in finite difference equation
g = acceleration due to gravity
G = gravitational parameter
h = grid spacing
H = total curvature of the free surface
k_N = iteration level in loop N
L_c = characteristic length
L_1 = length of the upstream region
L_2 = length of the downstream region
p = pressure
p_a = pressure in the surrounding medium
p_{ex} = exit pressure
r = transverse distance
R = profile describing the free surface

S = surface tension parameter
T = total stress
T_{mn} = components of total stress tensor
T_N = normal stress at the free surface
$(T_N)_{appl}$ = imposed normal stress at the free surface
T_t = tangential stress at the free surface
u = transverse velocity
v = axial velocity
v_m, v_n = components of velocity vector
V = average velocity
x_m, x_n = coordinate directions
Y = coefficient in finite difference equation
z = axial distance

Greek Letters

α = geometry indicator
β = velocity profile rearrangement factor
δ_{mn} = Kronecker delta
Δ = symbol in finite difference equation
ϵ_N = allowable error in loop N
η = transformed coordinate direction
μ = liquid viscosity
ξ = transformed coordinate direction
ρ = liquid density
σ = surface tension
τ_w = wall shear stress in Poiseuille flow
ϕ = arbitrary variable
ψ = stream function
ω = vorticity

Subscripts

ij = evaluation at grid node (i,j)
η, $\eta\eta$ = first and second derivatives with respect to η
ξ, $\xi\xi$ = first and second derivatives with respect to ξ

ACKNOWLEDGMENT

The authors would like to express their appreciation to the State University of New York at Buffalo for financial support.

LITERATURE CITED

Allan W., "Numerical Die-Swell Evaluation for Axisymmetric Tube Exits using Finite Element Method," *Intl. J. Num. Meth. Engr.*, **11**, 1621 (1977).

Bagley, E. B., and H. J. Duffey, "Recoverable Shear Strains and the Barus Effect in Polymer Extrusion," *Trans. Soc. Rheol.*, **14**, 545 (1970).

Batchelor, J., J. P. Berry, and F. Horsfall, "Die Swell in Elastic and Viscous Fluids," *Polymer*, **14**, 297 (1973).

Boger, D. V., and M. M. Denn, "Capillary and Slit Methods of Normal-Stress Measurements," *J. Non-Newt. Fluid Mech.*, **6**, 163 (1980).

Chang, P-W., T. W. Patten, and B. A. Finlayson, "Collocation and Galerkin Finite-Element Methods for Viscoelastic Fluid Flow—II," *Computers and Fluids*, **7**, 285 (1979).

Crank, J., and R. M. Furzeland, "The Numerical Solution of Elliptic and Parabolic Partial Differential Equations with Boundary Singularities," *J. Comp. Phys.*, **26**, 285 (1975).

Crochet, M. J. and R. Kuenings, "Die Swell of a Maxwell Fluid: Numerical Prediction," *J. Non-Newt. Fluid Mech.*, **7**, 199 (1980).

Daly, B. J., "A Technique for Including Surface Tension Effects in Hydrodynamic Calculations," *J. Comp. Phys.*, **4**, 97 (1969).

Davies, J. M., J. F. Hutton, and K. Walters, "A Critical Appraisal of the Jet-Thrust Technique for Normal Stresses with Particular Reference to Axial Velocity and Stress Rearrangements," *J. Non-Newt. Fluid Mech.*, **3**, 141 (1977).

Dutta, A., "A Theoretical Analysis and Experimental Study of Extrusion Blow Molding," Ph.D. Thesis, State University of N.Y./Bflo., Amherst, NY (1981).

Fischer, R-J., M. M. Denn, and R. I. Tanner, "Initial Profile Development in Melt Spinning," *Ind. Eng. Chem. Fund.*, **19**, 195 (1980).

Goren, S. L., and S. Wronski, "The Shape of Low-Speed Capillary Jets of Newtonian Liquids," *J. Fluid Mech.*, **25**, 185 (1966).

Gottlieb, M., and R. B. Bird, "Exit Effects in Non-Newtonian Liquids. An Experimental Study," *Ind. Eng. Chem. Fund.*, **18**, 357 (1979).

Graessley, W. M., S. D. Glassock, and R. L. Crawley, "Die Swell in Molten Polymers," *Trans Soc. Rheol.*, **14:4**, 519 (1970).

Harlow, F. H., and J. E. Welch, "Numerical Calculation of Time-Dependent Viscous Incompressible Flow of Fluids with Free Surface," *Phys. Fluids*, **8**, 2182 (1965).

Higashitani, K., H. Nishio, and I. Hara, "Velocity Profile Variation of a Viscoelastic Fluid Around a Die Exit," Proc. 7th Intl. Congress on Rheology, p. 478, Gothenburg, Sweden (1976).

Horsfall, F., "A Theoretical Treatment of Die Swell in a Newtonian Liquid," *Polymer*, **14**, 262 (1973).

Huang, D. C., and J. L. White, "Extrudate Swell from Slit and Capillary Dies: An Experimental and Theoretical Study," *Polym. Eng. Sci.*, **19**, 609 (1979).

Huilgol, R. R., and R. I. Tanner, "The Separation of a Second-Order Fluid at a Straight Edge," *J. Non-Newt. Fluid Mech.*, **2**, 89 (1977).

Lee, J-S., and Y-C. Fung, "Flow in Locally Constricted Tube at Low Reynolds Number, *J. Appl. Mech.*, **37**, 9 (1970).

Metzner, A.B., W-T. Houghton, R. A. Sailor, and J. L. White, "A Method for the Measurement of Normal Stresses in Simple Shearing Flows," *Trans. Soc. Rheol.*, **35**, 133 (1961).

Michael, D. H., "The Separation of a Viscous Liquid at a Straight Edge," *Mathematika*, **5**, 82 (1958).

Middleman, S., and J. Gavis, "Expansion and Contraction of Capillary Jets of Newtonian Liquids," *Phys. Fluids*, **4**, 355 (1961).

Nakajima, N., and M. Shida, "Viscoelastic Behavior of Polyethylene in Capillary Flow Expressed with Three Material Functions," *Trans. Soc. Rheol.*, **10**, 299 (1966).

Nickell, R. E., R. I. Tanner, and B. Caswell, "The Solution of Viscous Incompressible Jet and Free-Surface Flows Using Finite Element Methods," *J. Fluid Mech.*, **65**, 189 (1974).

Omodei, B. J., "Computer Solution of a Plane Newtonian Jet with Surface Tension," *Computers and Fluids*, **7**, 79 (1979).

———, "On the Die Swell of an Axisymmetric Newtonian Jet," *ibid*, **8**, 275 (1980).

Pearson, J. R. A., and R. Trottnow, "On Die Swell: Some Theoretical Results," *J. Non-Newt. Fluid Mech.*, **4**, 195 (1978).

Reddy, K. R., and R. I. Tanner, "Finite-Element Solution of Viscous Jet Flows with Surface Tension," *Computers and Fluids*, **6**, 83 (1978a).

———, "On Swelling of Extruded Plane Sheets," *J. Rheol*, **22**, 661 (1978b).

Richardson, S. "A Stick-slip Problem Related to the Motion of a Free Jet at Low Reynolds Number," *Proc. Camb. Phil. Soc.*, **67**, 477 (1970a).

———, "The Die Swell Phenomenon", *Rheol. Acta*, **9**, 193 (1979b).

Ruschak, K. J., "A Method for Incorporating Free Boundaries with Surface Tension in Finite Element Fluid-Flow Simulators," *Intl. J. Num. Meth. Eng.*, **15**, 639 (1980).

Silliman, W. J., and L. E. Scriven, "Slip of Liquid Inside a Channel Exit," *Phys. Fluids*, **21**, 2115 (1978).

———, "Separating Flow Near a Static Contact Line: Slip at a Wall and Shape of a Free Surface," *J. Comp. Phys.*, **34**, 287 (1980).

Sturges, L. D., "Die Swell: The Separation of the Free Surface," *J. Non-Newt. Fluid Mech.*, **6**, 155 (1979).

Tanner, R. I., "A Theory of Die Swell," *J. Polymer Sci*, **A-2, 8**, 2067 (1970).

Tanner, R. I., R. E. Nickell, and R. W. Bilger, "Finite-Element Methods for the Solution of Some Incompressible Non-Newtonian Fluid Mechanics Problems with Free Surfaces," *Comp. Meth. Appl. Mech. Eng.*, **6**, 155 (1975).

Thom, A., "The Flow Past Circular Cylinders at Low Speeds," *Proc. Roy. Soc. London*, **Series A, 141**, 651 (1933).

Thom, A., and C. J. Apelt, "Field Computation in Engineering and Physics," p. 130, D. van Nostrand Co., London (1961).

Thompson, J. F., F. C. Thames, and C. W. Mastin, "Automatic Numerical Generation of Body-Fitted Curvilinear Coordinate System for Fields Containing any Number of Arbitrary Two-Dimensional Bodies," *J. Comp. Phys.*, **15**, 299 (1974).

———, "Body-Fitted Curvilinear Coordinate Systems for Solution of Partial Differential Equations on Fields Containing any Number of Arbitrary Two-Dimensional Bodies," NASA-CR-2729, Washington, DC (1977).

Utracki, L. A., Z. Bakerdjian, and M. R. Kamal, "A Method for the Measurement of True Die Swell of Polymer Melts," *J. Appl. Polym. Sci.*, **19**, 481 (1975).

Vlachopoulos, J., M. Horie, and S. Lidorikis, "An Evaluation of Expressions Predicting Die Swell," *Trans. Soc. Rheol.*, **16:4**, 669 (1972).

Whipple, B. A., and C. T. Hill, "Velocity Distributions in Die Swell," *AIChE J.*, **24**, 664 (1978).

Manuscript received October 7, 1980; revision received April 13 and accepted April 23, 1981